Using IASI to detect the Deepwater Horizon Oil Spill

Jack Kemp

22nd October 2013

1 Introduction

On 20^{th} April 2010, the Deepwater Horizon oil rig at $28°44'17.30''$N and $88°21'57.40''$W in the Gulf of Mexico exploded and sank.[1] In the resulting oil spill, an estimated $780,000\ \text{m}^3$ of oil was released from the ocean floor, resulting in a slick which covered approximately $180,000\ \text{km}^2$ at its largest extent.[2] Figure 1 shows an image of the slick on the 24^{th} May 2010 taken from NASA's Terra satellite.

The Infrared Atmospheric Sounding Interferometer (IASI) is a Fourier Transform Spectrometer installed on the European meteorological satellite MetOp-A, which operates in the thermal infrared with spectral range 645–2760 cm^{-1}, sampling every $0.25\ \text{cm}^{-1}$.[4] In this project we attempted to use IASI to detect the increase in certain gases, particularly hydrocarbons, from the Deepwater Horizon spill and thus to measure its effect on air quality. We also investigated if the oil slick could be tracked directly from its impact on sea surface emissivity.

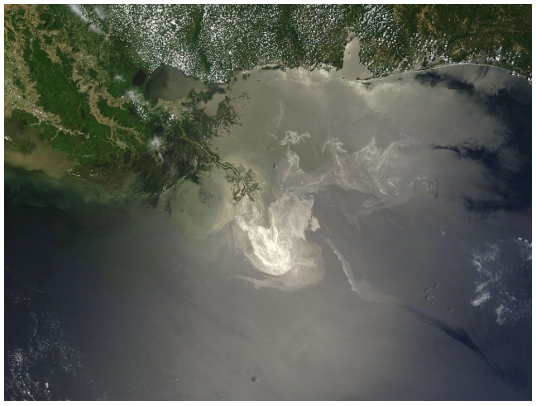

Figure 1: An image of the Deepwater Horizon oil spill taken from NASA's Terra satellite on the 24^{th} May 2010.[3]

2 Singular Value Decomposition

2.1 Method

The first method used was singular value decomposition (SVD). In brief, the SVD of an $n \times m$ matrix X yields three matrices: an $m \times m$ U, an $n \times n$ V, and a diagonal $n \times m$ matrix W.[5] The vectors which form the columns of V are called the **singular vectors** and the corresponding values of W are the **weights** of these singular vectors. If X represents a number of measurement vectors, for example IASI spectra, then the singular vectors represent the principal modes of variability of that data, while the weights are their relative importance for modelling the data.

It turns out that most of the variability of the data is contained within the first few singular vectors.[6] So if we fit these singular vectors to the original data using a linear regression, the residuals of the fit should merely be noise. If on the other hand we try a fit to some different data with some new component causing variability, the new component should make an impression on the residuals. The easiest way to check for and identify any new components then is to take the SVD of the residuals themselves and see whether there are any singular vectors of significant weight; if so then they can be used to identify the new components. If we then add these new singular vectors on to the original set and fit the data again, we can locate the new components in the areas where the fitting coefficients of the new singular vectors are large, as this is where they are needed to explain the variability.

2.2 Results

The training sets of data used were the brightness temperatures for the 15^{th} – 20^{th} April 2010 and 27^{th} May – 8^{th} June 2011, in a rectangle between latitudes 25°N and 28°53′24″N and longitudes 84°W to 92°W, covering an area of approximately $3.4 \times 10^5\,\text{km}^2$, see Figure 2. This includes the site of the rig itself but avoids coastal areas where additional variance would be present due to the land. As a test the first forty singular vectors of the SVDs of each of the two training sets were fitted to themselves and the residuals plotted. The residuals were simply noise as expected, although this was more obvious in spectral radiance space where they formed three levels of Gaussian noise corresponding to the three wavenumber ranges measured separately in IASI.

The fits and SVD of the residuals as described above were then applied to two data sets: one just after the spill on the 20^{th} – 30^{th} April 2010 and the other on the 27^{th} May – 8^{th} June 2010, after the effects of the spill had had time to build up. Firstly the training set just before the spill was used and several significant residual vectors were found, the first of which, with by far the most weight, is shown in Figure 3. Comparing the shape of this spectrum with known spectra suggested the possible influence of methane, ozone and carbon monoxide, which were searched for specifically (see below). However, locating where the singular vectors were needed

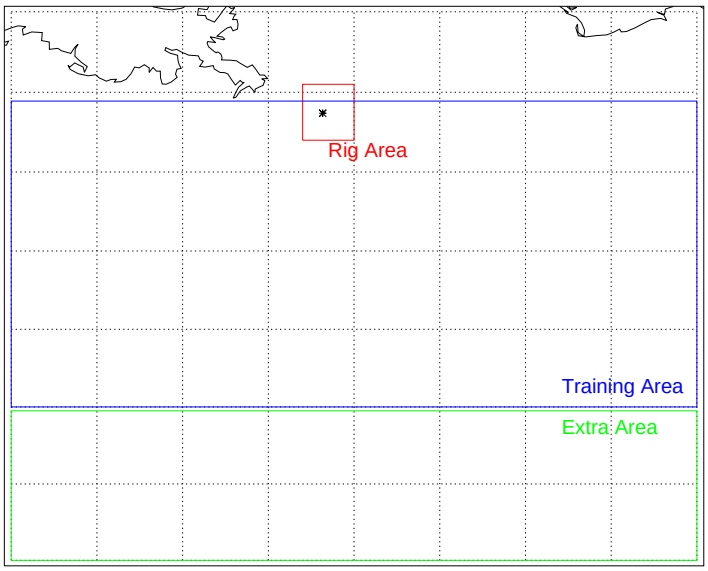

Figure 2: The areas used for the SVD fits. The star shows the location of the rigs.

as described above revealed no spatial coherence and certainly no clustering of large coefficients around the rig which would have indicated we had detected the spill. Worse, on applying the fit to the same date ranges and longitudes but further south between 23°N and 25°N, the fitting coefficients for the new singular vectors remained as large as they had by the spill. This, coupled with the fact that the coefficients tended to rise steadily as time went on, seemed to suggest that we were observing a seasonal effect.

This prompted using the second training set from the following year. Although the resulting residual singular vectors looked very similar, the trend upwards in time did decrease. However, there was still no spatial coherence and the fit continued to extend outside the region of the spill.

A smaller training set was used taking a small region around the rig, see Figure 2. Only one significant singular vector remained but this was the same as in Figure 3, albeit with slightly decreased weight.

At first the range of wavelengths was taken from 670–2300 cm^{-1} at the full IASI resolution of 0.25 cm^{-1}. However from Figure 3 it is clear that the ends of the singular vector are very noisy. Cutting these ends off and taking the range 800–2000 cm^{-1} instead, the fit from June 2011 to June 2010 was rerun. The weight of the first singular vector decreased greatly, suggesting much of the original variance came from the noise at these ends. The shape of the remaining singular vector did not

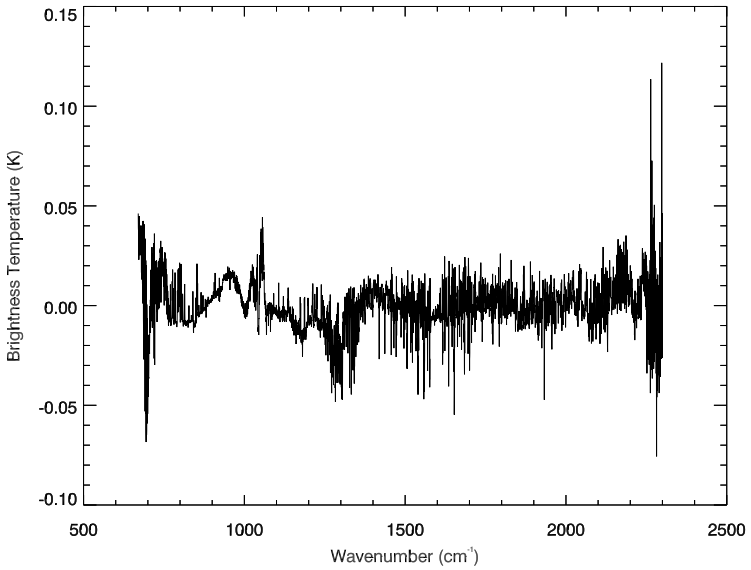

Figure 3: The first singular vector of the residuals for the April SVD fit to the June 2010 data. Notice the spectral features at around 1000 cm^{-1} and 1300 cm^{-1}, indicating the possible presence of increased ozone and methane.

change, however, and there was still no spatial coherence in the fitting coefficients.

The method was also tried for the wavenumber ranges 800–1150 cm^{-1} and 1150–1600 cm^{-1}. The weights further decreased, but when the fitting coefficients were plotted against one another there was found to be a correlation, suggesting there might be a true signal. However, the correlation could be due to shared seasonal effects, as both sets of coefficients shared a slight trend over time similar to that of mean brightness temperature in the window regions.

Lastly, the singular value decomposition was constructed for 100 cm^{-1} wide ranges between 800–1600 cm^{-1}. The only ranges with residual singular vectors with significant weight were 1200–1300 cm^{-1} and 1300–1400 cm^{-1}, and the fitting coefficients of these singular vectors were correlated. This suggested that there is one region of significance in the 1250–1350 cm^{-1} region, possibly representing methane.

3 Optimal Estimation for Specific Gases

Ship-borne air quality measurements taken after the spill on 8^{th} June 2010 show a large increase in the heavier hydrocarbons as well as ozone and carbon monoxide from the background Gulf of Mexico concentration.[7] As the singular vectors also hinted that there might be excess ozone, methane and carbon monoxide, we decided to look specifically for these gases to complement the more general SVD approach.

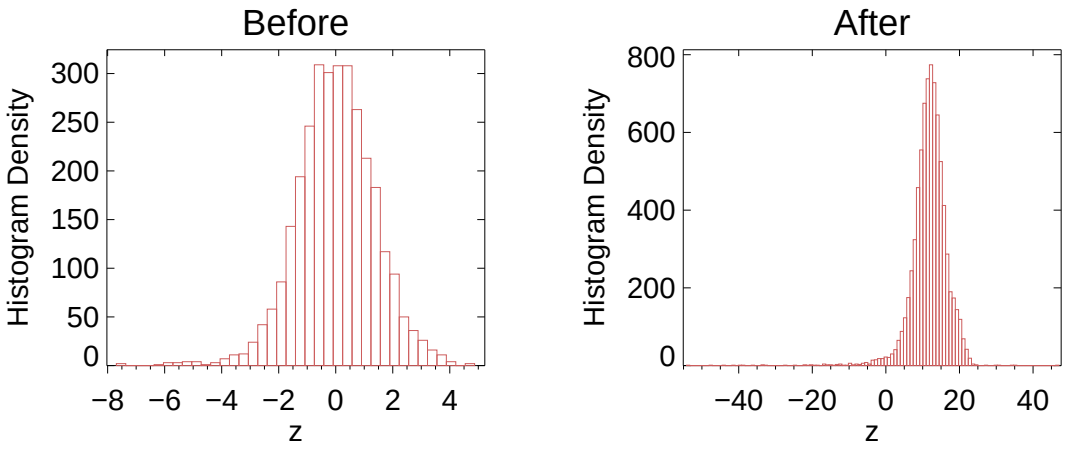

Figure 4: The histograms of carbon monoxide z values before and after the oil spill. We see that after the oil spill the distribution is significantly offset from zero.

3.1 Method

One method of doing this is outlined by J. C. Walker *et al.* in [8]. We suppose the measured spectrum $\mathbf{y}$ is related to the state vector of concentrations $\mathbf{x}$ via a forward model $F(\mathbf{x})$ and random and systematic error ϵ. Further we assume the forward model can be linearised about some normal climatological state vector $\mathbf{x}_0$, with Jacobian $\mathbf{K}(\mathbf{x} - \mathbf{x}_0)$ so that we may write:

$$\mathbf{y} - F(\mathbf{x}_0) = \mathbf{K}(\mathbf{x} - \mathbf{x}_0) + \epsilon.$$

This then leads to an optimal least-squares estimate for $\mathbf{x}$ of

$$\mathbf{z} = \mathbf{x} - \mathbf{x}_0 = \left(\mathbf{K}^T\mathbf{S}\mathbf{K}\right)^{-1}\mathbf{K}^T\mathbf{S}\left(\mathbf{y} - F(\mathbf{x}_0)\right),$$

where $\mathbf{S}$ is the total measurement error covariance matrix. This can be found by calculating the covariance of the measurements for a training data set which we do not expect to contain an excess or deficit of the gas in question, exactly like the training data sets for the SVD method. $F(\mathbf{x}_0)$, as the expected measurement of the spectrum with normal climatological concentrations of the gas, can then be replaced by the mean spectrum of the training set.

Lastly we need the Jacobian $\mathbf{K}$. We used the radiative transfer model the Reference Forward Model (RFM) [9] to calculate the expected spectrum for normal climatological conditions and then again with increased tropospheric concentrations of the gas in which we were interested; the difference between the spectra provided the column of the Jacobian relevant to our particular gas.

3.2 Results

The dates and areas used for the training data sets and the oil spill data sets were the same as for the SVD method. The specific gases searched for were ozone, methane, carbon monoxide, nitrous oxide, and propane. A histogram of the calculated z for carbon monoxide, which from above we see represents the difference between the measured and normal climatological concentrations of the gas, is shown in Figure 4. These histograms are typical of the results for all the gases. We see that in the training data set z is distributed as a Gaussian centred on zero, as we would expect, and that during the spill the mean value is offset from zero. This might suggest that we have detected an effect due to the spill. However as with the SVD method there is no spatial coherence to any of the larger or smaller values z, and again the offset also appears equally in areas outside the region affected by the spill. Furthermore plotting the methane and ozone coefficients out as a time series reveals the same increasing trend with time as suffered by the fitting coefficients of the first singular vector. This suggests that it is possible we are again viewing a seasonal effect.

4 Sea Surface Temperature and Emissivity

Oil has a lower emissivity in the thermal infrared than seawater. As a result, thick oil slicks appear warmer than the surrounding seawater during the day and cooler at night.[10] Hence one way to identify the oil slick would be to plot sea surface temperature and look for anomalies. A crude measure of sea surface temperature can be found from IASI by looking at the mean brightness temperature in the atmospheric window regions of the spectra. We attempted to remove clouds first, by taking a histogram of the mean brightness temperatures and cutting those much cooler than the mean value. Unfortunately, no obvious spatial coherence or difference between the temperature in June 2010 or June 2011 was observed. A time series of the temperatures from before and after the spill also did not reveal any effect from the spill.

As the oil is hotter by day and cooler by night, the area was gridded and in each grid the mean brightness temperature difference between day and night was calculated, in the hope that the oil slick would create regions of significantly greater difference. However, histogram plots of the day-night temperature difference with and without oil showed no noticeable difference between the two, nor was there any spatial coherence for the large differences even during the spill.

Lastly, the spectral emissivity of oil as a function of wavenumber in the 8–12 μm range is flat, whereas that of seawater decreases in the same range.[11] The RFM was run using a normal daytime atmosphere to find 30 channels centred on 8 μm and another 30 centred on 12 μm with over 99.5% transmissivity. The mean brightness temperature difference between these two groups of channels was then calculated per IASI pixel. Histograms of the differences in the June 2010 period

with the slick and the June 2011 without are shown in Figure 5. We see that as with most of the histograms without the slick the June 2011 histogram is centred on zero, whereas one would expect it to be negative, while on the other hand the June 2010 distribution is mostly negative. However, this change was also present in an area which should have been outside of the influence of the oil slick, nor was there any spatial coherence in anomalous brightness temperature differences around the slick. This again suggests we are viewing an effect not related to the oil slick itself.

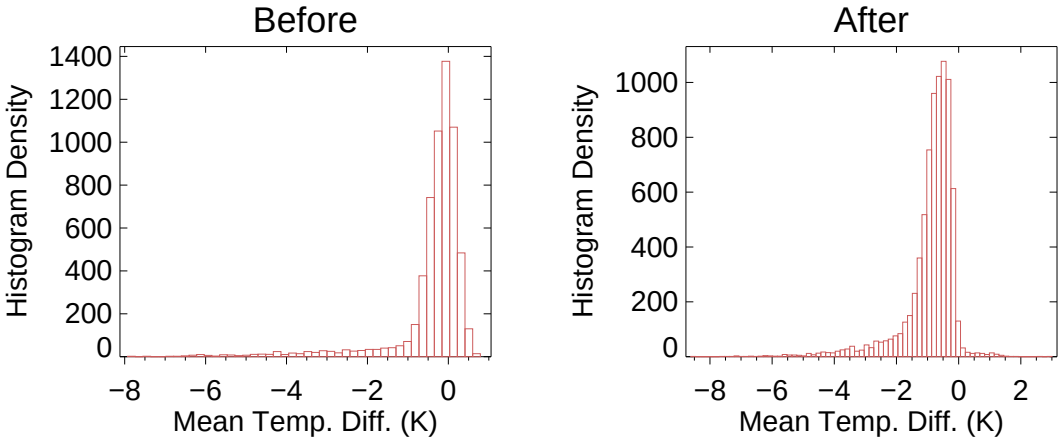

Figure 5: The histograms of mean brightness temperature difference between 30 channels around 8 μm and 12 μm for before and after the oil spill. Again, the after distribution is offset from zero.

5 Conclusion

We have examined the IASI data for the Deepwater Horizon oil spill using three main methods: singular value decomposition, optimal estimation of the concentration of likely gases, and sea surface temperature plots. While there have been hints of the oil slick from all three methods, in each case we have had to discount them due to a lack of any spatial coherence in the results, in particular no clustering around the site of the rig, and also because the effects appear outside of the area we expect the oil spill to have any influence.

The signal from the oil spill thus appears to be swamped by seasonal effects, even when a training data set from the same month the year after was used. This does not explain the lack of sea surface temperature results, but from a plot of sea surface temperature in the Gulf of Mexico, Figure 6, we can see that even without oil there is a large amount of variation in sea surface temperature anyway, so it is possible that the effect of the oil on sea surface temperature has been hidden behind these normal variations.

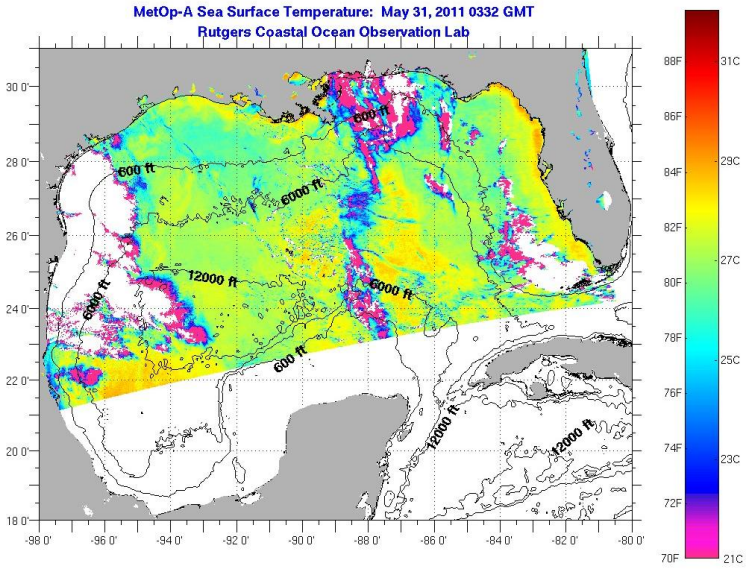

Figure 6: The sea surface temperature at 21:32 local time on the 30$^{\text{th}}$ May 2011.[12] Notice the complexity present even without the oil slick.

These problems are further compounded by the fact that the Deepwater Horizon oil spill was an *underwater* spill. This means that the oil may have moved away from the rig while rising to the surface, and despite covering a large area altogether may often have been a patchy, sub-pixel effect. This would have made it much harder to spot any spatial coherence from IASI. Furthermore, many of the lighter hydrocarbons such as methane would have dissolved on the way up, making the change in air quality harder to detect.

References

[1] NOAA/NESDIS, ERMA Deepwater Gulf Response [online], `http://gomex.erma.noaa.gov/erma.html`, last accessed 12 Aug. 2012

[2] B. Minchew, C. E. Jones, and B. Holt, 'Polarimetric Analysis of Backscatter From the Deepwater Horizon Oil Spill Using L-Band Synthetic Aperture Radar', *IEEE Transactions on Geoscience and Remote Sensing* (Oct. 2012), **50**:10, 3812–3829

[3] NASA, 'NASA's Terra Satellites Sees Spill on May 24', `http://www.nasa.gov/topics/earth/features/oilspill/20100525_spill.html`, last accessed 12 Aug. 2013

[4] D. Blumstein, G. Chalon, T. Carlier, C. Buil, P. Hebert, T. Maciaszek, G. Ponce, T. Phulpin, B. Tournier, D. Simeoni, P. Astruc, A. Clauss, G. Kayal, R. Jegou, 'IASI instrument: technical overview and measured performances', *Proceedings of the SPIE* (2012), **5543**, 196–207

[5] W. H. Press, S. A. Teukolsky, W. T. Vetterling, B. P. Flannery, *Numerical Recipes in C: The Art of Scientific Computing* (2nd ed., CUP: 2002), 59–66

[6] R. G. Grainger, D. M. Peters, G. E. Thomas, A. J. A. Smith, R. Siddans, E. Carboni, and A. Dudhia, 'Measuring Volcanic Plume and Ash Properties from Space', 12–13

[7] A. M. Middlebrook, D. M. Murphy, R. Ahmadov, E. L. Atlas, R. Bahreini, D.R. Blake, J. Brioude, J. A. de Gouw, F. C. Fehsenfeld, G. J. Frost, J. S. Holloway, D. A. Lack, J. M. Langridge, R. A. Lueb, S. A. McKeen, J. F. Meagher, S. Meinardi, J. A. Neuman, J. B. Nowak, D. D. Parrish, J. Peischl, A. E. Perring, I. B. Pollack, J. M. Roberts, T. B. Ryerson, J. P. Schwarz, J. R. Spackman, C. Warneke, A. R. Ravishankara, 'Air quality implications of the Deepwater Horizon oil spill', *PNAS* (11 Dec. 2012), **109**:50, 20280–20285

[8] J. C. Walker, A. Dudhia, E.Carboni, 'An effective method for the detection of trace species demonstrated using the Metop Infrared Atmospheric Sounding Interferometer', *Atmos. Meas. Tech.* (2011), **4**, 1567–1580

[9] A. Dudhia, 'Reference Forward Model', `http://www.atm.ox.ac.uk/RFM/`

[10] J. K. Buettner, C. D. Kern, 'The determination of infrared emissivities of terrestrial surfaces', *J. Geophys. Res.* (1965), **70**, 1329-1337

[11] J. W. Salisbury, D. M. D'Aria, F. F. Sabins Jr., 'Thermal Infrared Remote Sensing of Crude Oil Slicks', *Remote Sens. Environ.* (1993), **45**, 223–231

[12] Rutgers Coastal Ocean Observation Lab, 'Metop-A Sea Surface Temperature: May 31, 2011 0332 GMT', `http://marine.rutgers.edu/mrs/sat_data/show/?file=../../regions/gulfmexico/sst/noaa/2011/img/110531.151.0332.m02.jpg` last accessed 13 Aug. 2013